Intern rapport; IR 2004-02

KNMI

Retrieval of rain rate using AMSU measurements

Jarno Schipper

Koninklijk Nederlands Meteorologisch Instituut

De Bilt, 2004

Intern rapport; IR 2004-02

De Bilt, 2004

PO Box 201
3730 AE De Bilt
Wilhelminalaan 10
http://www.knmi.nl
Telephone +31 30 22 06 911
Telefax +31 30 22 10 407

Auteur: Schipper, J.

De reeks Intern rapport is in juli 2000 gestart en geeft bij afsluiting de vorderingen rond een project of instrument weer.
De inhoud is primair bestemd voor KNMI-ers, maar de publicaties zijn verder openbaar.
Lezers van buiten het instituut dienen er echter wel rekening mee te houden dat het gebruikte jargon niet in alle gevallen voor buitenstaanders duidelijk zal zijn.

Intern rapport

Retrieval of rain rate using AMSU measurements

Jarno Schipper

KNMI, De Bilt, 2004

Abstract

A method to remotely sense precipitation and classify its intensity over land surfaces is described. This method is intended to be used by KNMI in future. It is based on data obtained from the Advanced Microwave Sounding Unit (AMSU) onboard NOAA-15, -16 and -17 satellite. Since, this method is designed to work over different surface types, it mainly relies on the scattering signal of precipitation-sized particles received at very high frequencies. For the calibration and validation of the method a dataset of radar measurements obtained over the Netherlands. Results for the rain rate computed from the AMSU-B channels at 89 and 150 GHz. are compared with rain rate from Radar. It was found that rain rate from AMSU tends to overestimate the rain rate measured by Radar. A lack of correlation was found, and after calibration this lack of correlation was still present. Concluding that the rain rate from Radar could not be accounted for with AMSU. In addition to a statistical assessment of the method's accuracy, the case studies also help to demonstrate the capability of AMSU to detect rain. By applying a contingency table it shows that AMSU is successful in 20 % of the cases in identifying rain.

1. Introduction

The advanced microwave sounding unit (AMSU) was launched in May 1998 on board the NOAA 15 satellite. The AMSU is the second and most advanced microwave instrument launched by NOAA since the launch of the MSU instrument on board of TIROS-N satellite in 1978 (Grody *et al.,* 2001). The AMSU instrument contains 20 channels and is a replacement to the four-channel unit (MSU) and was primarily designed to obtain soundings, i.e., vertical profiles of atmospheric temperature and water vapour.

AMSU measures very low levels of microwave radiation naturally emitted by the Earth at different frequencies (or "channels"). The land, ocean, and atmosphere all have different emitting properties at different microwave frequencies. The amount of radiation measured by each AMSU channel is converted to a "brightness temperature". The brightness temperature of a substance is its real temperature multiplied by the substance's ability to emit radiation (its "emissivity"). For the AMSU frequencies, the emissivities range from about 0.4 (snow cover) to 0.5 (ocean) to 0.95 (dry land or vegetated land) to 1.0 for air. Each channel has a different mixture of sensitivities to these various features.

The AMSU consists of two instruments, AMSU-A and AMSU-B. AMSU-A is dedicated to derive information about the temperature profile, while the purpose of AMSU-B is mainly the retrieval of water vapour profile information.

Both the AMSU-A and AMSU-B instrument have window channels, which are most suitable to obtain information about precipitation. With AMSU-A these channels are measuring at 23.8, 31.4 and 89.0 GHz. AMSU-B contains two window channels at 89.0 and 150. GHz. These channels are least affected by water vapour or oxygen absorption, which makes them thus suitable for the retrieval of information about precipitation (Smith *et al.,* 1998).

The AMSU-A and AMSU-B instruments are cross-track scanning, where the AMSU-A consists of 30 measurements (step angle is 3.3°) and the AMSU-B consists of 90 measurements (step angle is 1.1°). So, during one AMSU-A measurement scan, three AMSU-B scans are performed. Both instruments are synchronized via a pulse at the beginning of each AMSU-A scan. The nadir effective field of view (EFOV) of AMSU-A varies between 50 x 48 km^2 at the scan center to 150 x 80 km^2 at the edge of the scan. AMSU-B measures with a higher spatial resolution of resolution of 1.1° and has a EFOV of about 20 x 16 km^2 at the scan center to about 64 x 52 km^2. These details can be found in (Goodrum *et al.,* 1999) and (Bennartz, 1999).

In 2002 Zhao and Weng (2002) developed an algorithm to simultaneously derive cloud ice water path (IWP) and particle effective diameters (D_e) using AMSU-B window measurements from 89 and 150 GHz. In their research they discovered that the AMSU-B derived IWP and D_e are strongly correlated to the features of surface rainfall under most weather conditions. Due to this relationship between IWP and rain rate, IWP was converted into rain rate through validation with MM5 cloud model data. However, problems persisted because the retrieved rain rate tended to overestimate stratiform and underestimate convective precipitation. More research by Ferraro *et al.,* (2003) was done to deal with this problem. A postlaunch calibration scheme was developed and parameters like the convection index (CI) were build into the algorithm to reflect the convection strength of precipitation systems. The algorithm to retrieve IWP was validated with data obtained from a series of Special Sensor Microwave/Imagers (SSM/I) and in 2003 the algorithm to retrieve rain rate from AMSU-B measurements was updated after validation with data obtained through NCEP (Ferraro *et al.,* 2003).

Precipitation is one of the most difficult meteorological variables to measure (Weng *et al.,* 2003). The networks of rain gauges over populated continents provide poor sampling and over areas with deserts and densely forested areas there is hardly any data available concerning rain rate. Over oceans they are almost nonexistent. By using AMSU measurements it could be possible to collect data of rain rate. At

KNMI there is interest in researching the possibilities to determine rain rate from AMSU measurements. Since the conversion of IWP to rain rate will also have some regional dependence based upon the physical process of the precipitation regime we need to validate the algorithm that retrieves rain rate with data obtained through Radar.

In chapter 2 the algorithm to retrieve the ice water path (IWP) and rain rate (RR) will be discussed, followed by a description of the data used in this research, in Chapter 3. The results will be shown, compared and validated with Radar in Chapter 4. A discussion about these results will be given in Chapter 5. A conclusion concerning this research will be given in Chapter 6.

2. Methodology

In this chapter a description will be given about the methodology that is presented in literature (Zhao and Weng, 2002; Ferraro *et al.,* 2003) to retrieve the rain rate (RR) from AMSU-B measurements. Three distinguishing steps can be identified and by simplifying these three steps the algorithm to retrieve RR can be described as follows;

1. The effective diameter (D_e) of ice particles is computed using AMSU measurements.

2. By using the brightness temperatures at cloud base and cloud top, which are obtained through AMSU measurements, the Ice Water Path (i.e. related to the number of ice particles with size D_e) can be derived.

3. The derived Ice Water Path (IWP) is then converted into the surface rainfall rate through an IWP and rainfall rate relationship which was developed from cloud model results.

By looking at these three steps it makes it easy to understand how the retrieval of RR functions. In the first step the size of the ice particles is computed. The second step contains the computation of the Ice Water Path. In this step the number of ice particles, with size D_e, that are present in a cloud are computed. By now information about the number of ice particles (IWP) and the size of the ice particles (D_e) are known and in the final step this information is converted to RR.

These three steps help us in understanding the algorithm to retrieve RR. In the following paragraphs a more thorough description will be provided about the retrieval of D_e, IWP and RR.

2.1 Retrieval of D_e and IWP

The earth's atmosphere contains various types of particles ranging from aerosols, water droplets, and ice crystals to raindrops, snowflakes and hailstones. They are produced by a number of physical and dynamical processes, which govern their formation and growth in the atmosphere. For the retrieval of the rain rate we are only interested in the particles that exist within a cloud. Clouds are composed of water droplets and/or ice particles. The microphysical state of a cloud is determined by the dispersion of particles sizes and the phase (ice or liquid). A typical value for a water droplet is in the order of 5 μm (Liou, 2002). Some middle clouds with temperatures warmer than –20 °C contain supercooled water droplets that coexist with ice particles. Larger droplets (20 μm) can grow by collision and coalescence and produce millimeters of rain, which is evident from our daily experience. At the AMSU lower frequencies the scattering from cloud liquid is however neglected. For AMSU ice particles are the most important to the contribution of rain. Ice crystals in the atmosphere are primarily present in cirrus clouds, as well as in the top portion of some middle clouds. The formation, maintenance, and dissipation of cirrus clouds are associated with large-scale synoptic features and disturbances. The shape of the ice particles depend on the temperature and relative humidity as well as whether they undergo collision and coalescence processes in the clouds. Because ice crystal size and shape vary greatly with time and space (Liou, 2002), a presentation of representative is a difficult task. Nevertheless, typical ice-crystal size distributions for midlatitude cirrus clouds have been developed on the basis of a number of observations. The mean ice crystal effective size (diameter) can be defined by:

$$D_e = \frac{\int_0^\infty N(D)D^3 dD}{\int_0^\infty N(D)D^2 dD} \tag{2.1}$$

In equation 2.1 $N(D)$ depicts the particle size distribution function, D^3 is defined as the volume of an ice crystal, and D^2 is the geometric projected area of an ice crystal on a surface perpendicular to the incident beam (Weng and Grody, 2000). From this equation the Ice Water Contents (IWC) can also be easily derived when the volume of the ice particles is multiplied with the bulk density of ice (ρ_i). For a given ice crystal size distribution IWC is defined as:

$$IWC = \int_0^\infty D^3 \cdot \frac{\pi}{6} \rho_i dD \tag{2.2}$$

The Ice Water Path (IWP) follows from this equation if the IWC is multiplied by the difference in height between cloud top and base (Δz);

$$IWP = IWC \cdot \Delta z \tag{2.3}$$

The equations 2.1, 2.2 and 2.3 do give us a more physical understanding of the parameters D_e, and IWP, which are important for the retrieval of the rain rate. However, in practice these equations are of no use since AMSU does not measure the diameter or the number of ice particles, unlike for instance Radar. Weng and Grody (2000) proposed an alternative algorithm to derive both IWP and D_e using dual millimeter wavelength measurements. They found that for a given particle bulk volume density, the brightness temperature at millimeter-wave frequencies can be uniquely related to IWP and D_e. This relationship is expressed by the brightness temperatures emanating between cloud base, $T_B(z_b,\mu)$ and cloud top, $T_B(z_t,\mu)$. Which can be expressed as:

$$T_B(z_t,\mu) = \frac{T_B(z_b,\mu)}{1+\Omega(\mu)} \tag{2.4}$$

where Ω is the scattering parameter of the ice cloud; z_t and z_b are the heights of the cloud top and base, respectively; μ is the cosine of the zenith angle. The brightness temperature $T_B(z_t,\mu)$ in equation (2.4) decreases as the scattering parameter Ω increases. In equation (2.4) Ω is the most important parameter and is defined as:

$$\Omega(\mu) = \frac{1}{2\mu}(1-\omega g)\tau \tag{2.5}$$

Where τ is the ice cloud optical thickness, g is the asymmetry factor and ω is the single scattering albedo (Weng and Grody, 2000). Changes in ice water path and/or particle size in ice clouds will result in a variation of the scattering parameter. Therefore, the influence of ice cloud microphysical parameters on microwave measurements can be quantitatively analysed using equations (2.4) and (2.5). In particular, the scattering parameter can be related to the cloud ice water path and particle size through the optical thickness, which is defined as:

$$\tau = \int_{z_b}^{z_t} dz \int_0^\infty \frac{\pi}{4} D^2 Q_{ext} N(D) dD \tag{2.6}$$

In equation 2.6 Q_{ext} is depicted as the extinction efficiency of ice particles. For spherical ice particles with the size distribution $N(D)$, IWP can now be expressed as:

$$IWP = \int_{z_b}^{z_t} dz \int_0^\infty \frac{\pi}{6} D^3 \rho_i N(D) dD \tag{2.7}$$

For ice particles distributed according to a gamma function, Ω can be calculated with Mie theory (Ulbrich, 1983) and is expressed as a function of cloud ice water path (IWP), particle effective diameter (D_e), and particle bulk volume density (ρ_i) as follows:

$$\Omega(\mu) = \frac{IWP}{\mu \rho_i D_e} \Omega_N \tag{2.8}$$

Where Ω_N is the normalized scattering parameter, which is dependent only on the particle effective size D_e. When equation 2.8 is rearranged the cloud ice water path can be derived:

$$IWP = \mu \cdot \rho_i \cdot D_e \frac{\Omega}{\Omega_N} \tag{2.9}$$

When the upwelling brightness temperature at the cloud base is known, Ω can also be determined through equation 2.4:

$$\Omega(\mu) = \frac{T_B(z_b, \mu) - T_B(z_t, \mu)}{T_B(z_t, \mu)} \tag{2.10}$$

If we look at equation 2.8 we see that IWP is directly proportional to Ω. However, the relationship between Ω_N and D_e is non-linear and may depend on the particular ice particle size distribution $N(D)$ and bulk volume density (ρ_i). Therefore measurements at two distinct frequencies normally are required to determine both IWP and D_e. For AMSU these measurements are the 89 and 150 GHz. channels. It are these channels that are most affected from water vapour. Provided that the bulk volume density of ice particles can be determined from other sources independently (i.e., assumed to be either a constant or a function of ice particle size), the IWP essentially only depend on the scattering parameter Ω. Because most published bulk density-size relations are derived for ice particles in nonprecipitating cirrus clouds, there are some uncertainties in using these relationships in the retrieval because the AMSU measurements are primarily sensitive to the precipitating ice clouds. Thus, a constant density of 600 $kg\ m^{-3}$ is used in this study. The retrieval errors due to the uncertainties of bulk volume density are studied and presented in Chapter 5.

Between the scattering parameter ratio of two channels (89 and 150 GHz.) and D_e an empirical relation exists (Weng, 1992). This relation evolves from a Taylor-series. The ratio (r), between Ω_{89} and Ω_{150} is defined and used here to determine D_e (Eq. 2.11) by eliminating IWP and assuming a modified gamma distribution (Zhao and Weng, 2002), that is;

$$r = \frac{\Omega_{89}}{\Omega_{150}} \tag{2.11}$$

where Ω_{89} is equal to:

$$\Omega_{89} = \frac{BT_{89} - T_{89}}{T_{89}} \tag{2.12}$$

and Ω_{150} equals:

$$\Omega_{150} = \frac{BT_{150} - T_{150}}{T_{150}} \tag{2.13}$$

T_{89} and T_{150} are the brightness temperatures at cloud top, measured with AMSU-B at 89 and 150 GHz, respectively. In equation 2.12 and 2.13, over land the brightness temperature at cloud base (BT_{89} and

BT_{150}) can be determined from measurements from AMSU-A at 23 and 31 GHz (Zhao and Weng, 2001; Fig 2.1).

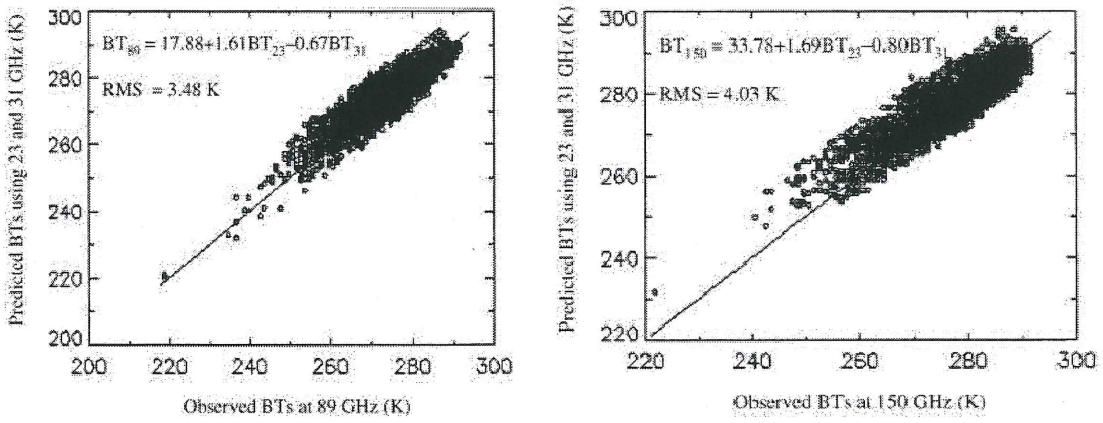

Fig 2.1. Regression relationship that is derived to estimate the cloud-base brightness temperatures BT_{89} (left) and BT_{150} (right) using the measurements of AMSU-A at 23 and 31 GHz (Zhao and Weng, 2001).

Over land, the cloud-base brightness temperature is estimated using an empirical relationship that exists between the AMSU lower and higher frequencies (Fig. 2.1). In order to retrieve the brightness temperatures at cloud base at 89 and 150 GHz, Zhao and Weng (2001) derived the following relationship;

$$BT_{89} = 17.88 + 1.61BT_{23} - 0.67BT_{31} \tag{2.14}$$

and

$$BT_{150} = 33.78 + 1.69BT_{23} - 0.80BT_{31} \tag{2.15}$$

As shown in Figure 2.1, the brightness temperatures of 89 and 150 GHz are estimated with a root mean square (rms) error of about 4.0 K. This implies that the brightness temperature depressions at 89 and 150 GHz must be greater than 4.0 K to still be able to identify clouds reliable. Which means that Ω_{89} must be greater than 0.01, since an rms of 3.48 divided by 260 K is 0.01. A value smaller is considered not reliable. For Ω_{150} the value should be greater than 0.02 to be considered reliable.

The scattering parameter ratio ideally varies between 0 and 1. For ice clouds having small ice particles, Ω_{89} nearly vanishes and the ratio approaches 0. For ice particles having a larger effective diameter, the scattering parameter ratio approaches unity when the scattering intensities at 89 and 150 GHz reach their geometrical optical limit. An empirical relationship between r (Eq. 2.11) and D_e was derived using simulated data from a radiative transfer model (Weng, 1992).

$$D_e = a_0 + a_1 r + a_2 r^2 + a_3 r^3 \tag{2.16}$$

In this equation the a_i (i = 0, 1, 2, 3) are regression coefficients which are dependent on the ice particle bulk density and the size distribution. These coefficients are presented in Table 2.1. The effective particle diameter randomly varies within a range of 0.1–3.5 mm. The ratio initially increases as D_e increases and then approaches to a constant when ice particle effective sizes become very large. For small D_e (<0.4 mm), the scattering parameter of 89 GHz is small because of its lack of sensitivity to the small-size ice particles. Therefore, the size information cannot be determined uniquely by the scattering parameter ratio of 89 and 150 GHz. For D_e between 0.4 and 2.5 mm, Ω_N at both 89 and 150 GHz linearly increases with D_e, and Ω_N at 150 GHz is much higher than that at 89 GHz. However, for a larger D_e (greater than 3.5 mm), Ω_N at both frequencies tends to approach to the same constant value.

The minimum detectable ice particle size is about 0.5 mm for 89 GHz. With the dual-frequency measurements at 89 and 150 GHz, reliable results are expected when the ratio ranges from 0.2 to 0.8.

The regression relations of Ω_N - D_e are obtained from data as follows:

$$\Omega_N = \exp\{b_0 + b_1 \ln(D_e) + b_2 [\ln(D_e)]^2\} \quad (2.17)$$

As mentioned earlier the relationship between Ω_N and D_e is non-linear and depends on the particular size distribution and bulk volume density, unlike the scattering parameter Ω presented in equation 2.10, which only depends on the brightness temperatures of cloud top and base. The relationship between Ω_N and D_e is represented through the regression coefficients b_i (i = 0, 1, 2) which are listed in Table 2.1.

Table 2.1. List of the regression coefficients used in the Ω_N and D_e equations (Ferraro *et al.*, 2003).

D_e	a_0	a_1	a_2	a_3
	-0.300323	4.30881	-3.98255	2.78323
		b_0	b_1	b_2
Ω_N	$D_e \leq 1$ mm	-0.294459	1.38838	-0.753624
	$D_e > 1$ mm	-1.19301	2.08831	-0.857469

When the brightness temperatures at ice cloud base are estimated with equation 2.14 and 2.15, the scattering parameter ratio can be computed using equation (2.11) with satellite measurements from two frequencies (89 and 150 GHz.) Thus, D_e can be determined unambiguously from equations (2.16), (2.17), and (2.11) for a given bulk volume density. The IWP can be determined using equation 2.9, however information about the cloud base temperature is needed in order to retrieve the scattering parameter Ω (Eq. 2.10). Ferraro *et al.*, (2003) derived the following relation between the scattering parameters Ω_{89} and Ω_{150} to estimate Ω;

$$\Omega = \frac{\Omega_{150} - \Omega_{89}}{\Omega_{89}} \quad (2.18)$$

Given the ice particle bulk density, IWP ($kg\ m^{-2}$) can then be uniquely determined (2.9).

2.2 Retrieval of the Rain Rate, RR

The relationship between the surface rain rate and ice water path is derived using the Goddard precipitation profiling algorithms (Kummerow *et al.*, 1996, Ferraro *et al.*, 2003).

$$RR = a_0 + a_1 IWP + a_2 IWP^2 \quad (2.19)$$

Where IWP is the ice water path. Three new regression coefficients are introduced; a_0, a_1, a_2. These coefficients depend on the precipitation regime, which is expressed by a convective index (CI). Depending on this convective index, rain rate is computed using different coefficients (note Table 2.2).

2.3.1 Retrieval of the Convective Index, CI

As was mentioned, the regression coefficients in equation 2.19 depend on the convective index (CI). This was done because the retrieval of the rain rate using IWP tended to overestimate stratiform precipitation and underestimate convective precipitation. By making discrimination between the convectivity of the regime in the form of a CI and adjusting the regression coefficients an attempt is made to overcome the problem of overestimation and underestimation of stratiform and convective precipitation, respectively. The CI can be derived using measurements of AMSU-B. The AMSU-B 183 GHz moisture channels are sensitive to the interaction of cloud ice and water vapour, which produce variations in the upwelling brightness temperature variations (Zhao *et al.*, 2003). The

convective index (CI) (e.g., weak, moderate and strong) is computed by using the three 183 GHz channels by examining differences between them. In Figure 2.2a the lowest brightness temperatures (BT) at the three 183 channels are plotted against the longitude. Figure 2.2b shows the BT at 150 GHz. Figure 2.2a shows that the 183±7 GHz channel is the first to detect the ice scattering among the three since it is able to view deeper into the layer of scattering than the 183±1 GHz channel. The scattering signature of the ice particle at 183±1 GHz only becomes more visible as ice particles are brought up to higher altitude by the strong updraft motion (shown in Figure 2.2b as very cold region). Therefore, the brightness temperature difference of various 183 GHz channel pair might imply the convective strength that relates to ice particles in the cloud, and also indicates the height that ice particles possible exist.

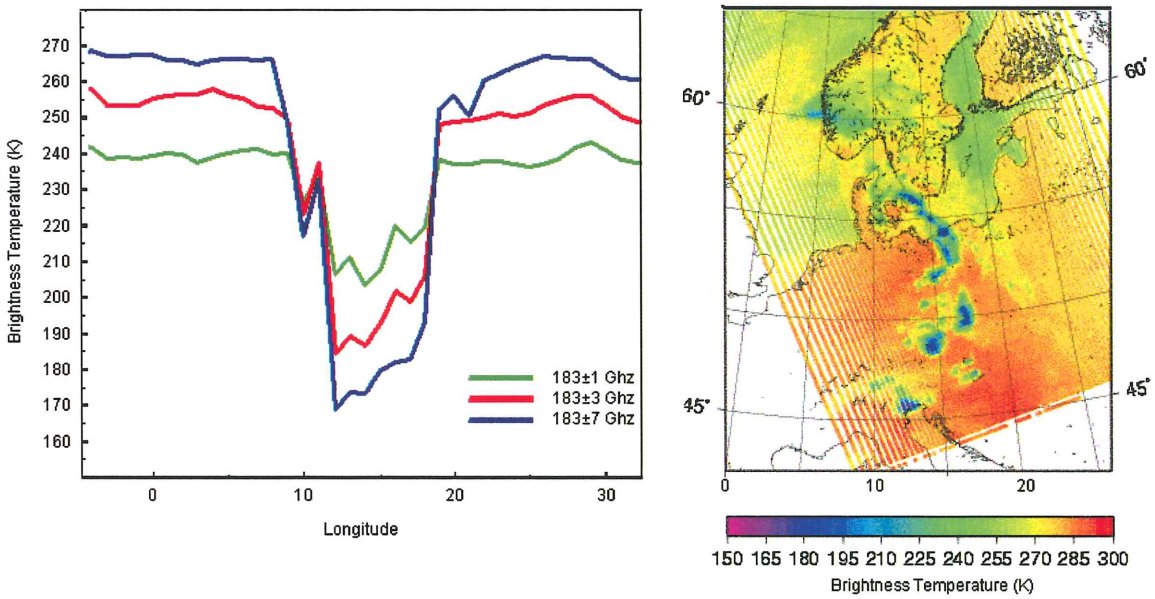

Fig 2.2a (left) Observed brightness temperatures at the 183 Ghz windows channels at June 26th, 2003. **Fig. 2.2b** (right). Observed brightness temperature at 150 Ghz, at June 26th, 2003.

The convection index (CI) which reflects the convection strength of precipitation systems, is calculated using the AMSU-B moisture channels (183±1, 183±3 and 183±7) as follows:

CI = 1 for $\Delta 2 > -2$ and $\Delta 2 > \Delta 1$ and $\Delta 2 > \Delta 3$
CI = 2 for $\Delta 2 > 0$ and $\Delta 1 > 0$ and $\Delta 3 > 0$ and $\Delta 1 > \Delta 3$ and $\Delta 2 > \Delta 3$
CI = 3 for $\Delta 2 > 0$ and $\Delta 1 > 0$ and $\Delta 3 > 0$ and $\Delta 1 > \Delta 3$ and $\Delta 2 < \Delta 3$

Where $\Delta 1$ = 183±1 - 183±7 , $\Delta 2$ = 183±3 - 183±7 and $\Delta 3$ = 183±1 - 183±3 and the values for CI of 1, 2 and 3 represent weak, moderate and a strong convection, respectively. Depending on these convective indices, rain rate is computed using different coefficients (note table below).

Table 2.2. List of the regression coefficients used to retrieve RR (Ferraro *et al.,* 2003).

	a_0	a_1	a_2
CI = 1 or 2	0.321717	16.5043	-3.3419
CI = 3	0.08925	20.8194	-2.9117

2.3 Screening procedure

The scattering signatures resulting from desert, ocean, ice and snow particles at higher microwave frequencies are similar to that of the ice particles because the dielectric constants among these scatters are almost the same (Zhao and Weng, 2001). It is thus important to eliminate this surface scattering in order to prevent calculating the rain rate wrongly. Including these surfaces will cause an

overestimation of the rain rate. AMSU alone does not provide enough information about surface types, however with AMSU-A it is possible to remove the surface scattering from sea ice and snow by using the low frequencies of AMSU-A. In order to remove surface scattering from desert areas (desert areas also scatter at 89 and 150 GHz) one can use measurements from AMSU-B at 183±7 GHz. It is this channel that peaks in the lower troposphere and is less affected by the surface (Weng *et al.,* 1997). Other screening procedures include discrimination in land and sea. The calculation of the scattering parameters over sea are much different to that over land. In this study we however will only look at the rain rate over land, since for the validation, we only have data from radar available over land. In Chapter 5 we will discuss the calculation of rain rate over sea in further detail.

Other screening procedures used in the algorithm are shown in Figure 2.3.

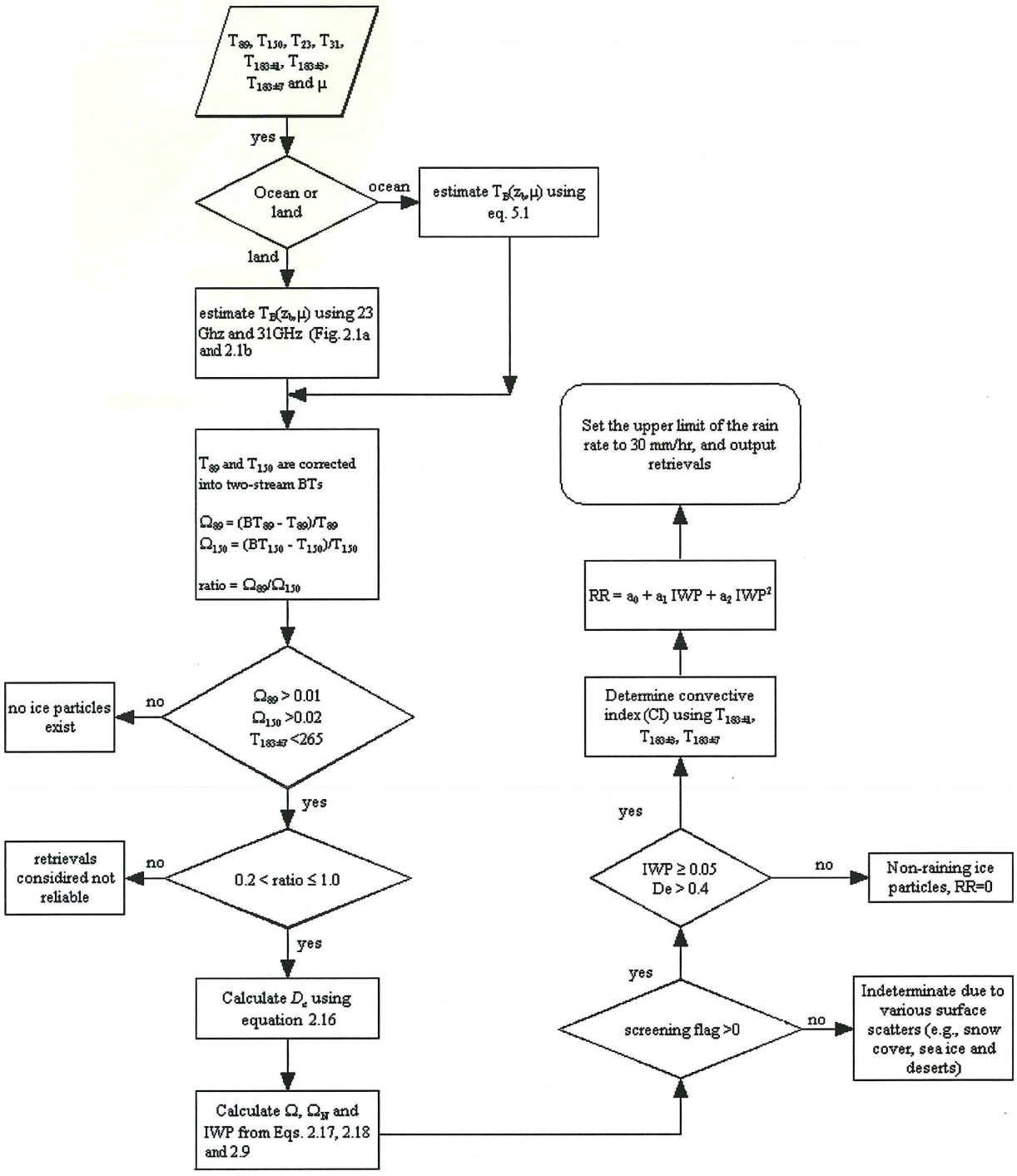

Fig. 2.3 The flow diagram of the AMSU-B rain rate algorithm

3. Data

Most information concerning the data and the products that could be derived from AMSU were handled in the previous two chapters. The procedures to calculate the rain rate from AMSU-B also include data obtained through AMSU-A (see section 2.1). The spatial difference in resolution between latter two however can cause problems. This chapter will describe these problems and what procedures were followed in order to avoid them.

Beside data from AMSU, also data obtained from Radar is used for validation of the rain rate. A description following this data will be given in this chapter.

3.1 AMSU

The AMSU consists of two instruments, AMSU-A and AMSU-B. Both instruments are cross-track scanning. The AMSU-A consists of 30 measurements along a scan line and AMSU-B does 90 measurements along a scan line. Due to this difference in resolution problems occur when solving equations 2.7 and 2.8. For these equations information from AMSU-A, 23 and 31 GHz channels is needed in order to calculate the scattering parameters at 89 and 150 Ghz.

A program in C-language was written (Appendix A) in which the first step was to calculate the brightness temperature at cloud base for 89 and 150 GHz using the 23 and 31 GHz windows channels (eq. 2.14 and 2.15). By doing this one ends up with a grid on AMSU-A resolution with all these BT_{89} and BT_{150}'s. Second step is to calculate the distances between every AMSU-B and AMSU-A using the latitudes and longitudes of the pixel. When the smallest distance was found it would continue to calculate Ω_{150}, Ω_{89} and subsequently the RR.

Due to the computational time involved, this procedure was made more efficient by using the last value for AMSU-A and the eight surrounding AMSU-A pixels to calculate the distance for the next AMSU-B pixel. For example:

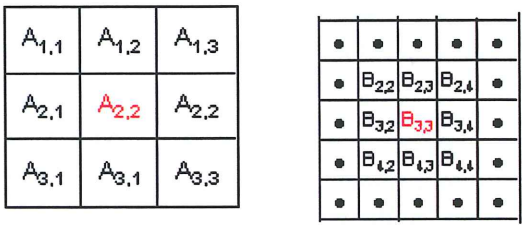

Fig. 3.1 AMSU-A grid (left) and AMSU-B grid

When calculating the closest distance from AMSU-B pixel $B_{3,2}$ we found out that AMSU-A pixel $A_{2,2}$ was the closest. The position of this pixel will then be stored in computer memory. When calculating the smallest distance of $B_{3,3}$ to AMSU-A we will use the stored value for AMSU-A ($A_{2,2}$) and the pixels surrounding this stored AMSU-A pixel to calculate the distance. By applying this procedure we can reduce the number of calculations.

For a further processing of the AMSU data to rain rate and the validation of this rain rate, three cases were chosen from the dataset with AMSU data of 2003. These three cases were chosen after analysing the daily sums of precipitations. Radar images that were coincident with AMSU overpasses were provided by KNMI. The date and the time of the cases studies used in this study are:

04-26-2003 at 10:25 UTC, 05-05-2003 at 10:25 UTC and 09-10-2003 at 10:45 UTC.

3.2 Radar

The data used in this study to validate the calculated rain rate from AMSU-B is measured by Radar. Currently two radars are operational, one in De Bilt and one in Den Helder. The Radars emit and receive Radio-waves with a frequency of about 6 GHz and with a wavelength close to 5 cm. The measurements received from Radar are, after some calibration and correction for the distance, converted to a quantity Z, the so-called Radar reflectivity (Holleman, 2003). With the assumption that the diameter (D) of the scattering precipitation particles are smaller than the wavelength of the Radar radiation, the assumption is made that Rayleigh scattering is dominant. The quantity, Z can subsequently be related to the size distribution of the raindrops in the radar sample volume according to (Doviak and Zrnić, 1993):

$$Z = \int_0^\infty N(D) D^6 dD \tag{3.1}$$

Where $N(D)$ is the drop size distribution, and D is the diameter of the droplet. Although Z is called the radar reflectivity factor, it is a purely meteorological quantity that is independent of any radar property. Because in practice the variations in radar reflectivity may span several orders of magnitude, it is often convenient to use a logarithmic scale. The logarithmic radar reflectivity is defined as Z and is expressed in units of *dBZ* (Doviak and Zrnić, 1993).

When the above equation and relations are combined and empirically tuned to the observations, the result is a formula for converting radar echo intensity in *dBZ* to rainfall rate. At KNMI the following equation is used to convert radar reflectivity into precipitation rate:

$$Z[dBZ] = 23 + 16 \cdot {}^{10}\log \mathrm{RR} \tag{3.2}$$

Where RR is the rain rate in mm hr^{-1}.

The reflectivity is measured at a large distance from the Radar (0~320 *km*) at a moderate altitude (0.8~7 *km*) above the surface of the earth; therefore discrepancies can occur between the precipitation rates as determined using the Radar and those determined by the on-ground observers (Holleman, 2003). This can be caused by, for instance, evaporation or generation of precipitation just above the earth's surface or by anomalous propagation of the Radar beam. From results of the radar verification, however, it was concluded that up to a distance of ~150 *km* the KNMI Radars produce a rather good quantitative view of the precipitation (Holleman, 2003).

From the time and dates of the case studies that were chosen from the AMSU data (see section 3.1) the corresponding data from Radar was gathered.

4. Results

To validate the AMSU-B rainfall rate, the rainfall measured by Radar is used as reference. The Radar rain rate is first projected onto a AMSU-B grid with the same set of map projection parameters. Because of the difference in resolution one will find more Radar pixels corresponding to one AMSU-B pixel. To overcome the difference in resolution a similar procedure as presented in section 3.1 is used. The measured rainfall data from Radar, closest to AMSU-B observations, are selected. Only the highest values of the rain rates of these Radar pixels are then selected. By doing so, a grid-to-grid match-up between Radar hourly rainfall data and AMSU-B estimates of rain rate is generated (Fig. 4.1; for the procedure see Appendix B). Finally the values of the Radar pixels were multiplied with a land mask. By doing this the values of the rain rate above sea can be filtered out of the data set.

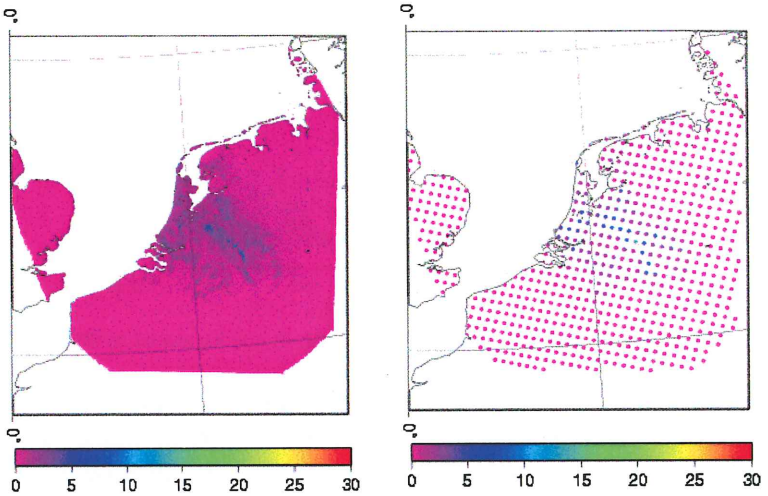

Fig. 4.1 The transformation from rain rate from Radar to AMSU-B grid on 9-10-2003, with rain rate in mm h^{-1}.

The final step will be to compare the rain rate estimated from AMSU-B with measured hourly rainfall by Radar to validate them.

4.1 Validation

For the calculations of the rain rate using AMSU-B equation 2.19 was used. The values for the regression factors were given by Ferraro *et al.,* (2003) and resulted after a validation with NCEP Stage IV data. The computation of the rain rate with this algorithm can be seen in Figure 4.2 (left). For comparison the rain rate obtained through Radar is plotted next to it in this Figure (right).

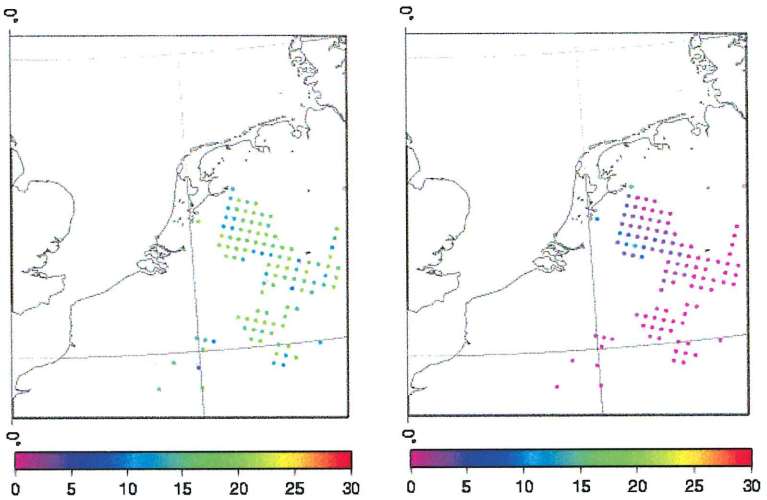

Fig. 4.2 Rain rate calculated by AMSU-B (left) and measured by Radar (right) on 9-10-2003 at 10:45 UTC, with rain rate in mm h^{-1}.

At this first stage it is already obvious from Figure 4.2 that there is a difference between the two methods in reference to their rain rate. This difference in rain rate is also present on both the other two days. Combining the case studies the difference and the poor correlation between the two methods can also be observed from Figure 4.3.

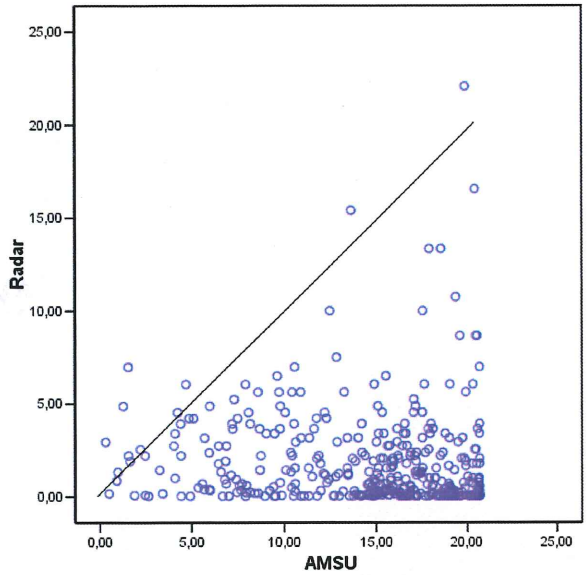

Fig. 4.3. Scatterplot of the rain rate estimated by AMSU-B and measured by Radar, in mm h^{-1}.

In Figure 4.3 the rain rates from Radar and AMSU-B are plotted. Beside the lack of correlation we can also see that AMSU overestimates the rain rate in comparison to Radar (most values are below the 1:1 line). The case studies are all characterized by a stratiform precipitating regime, and one of the problems with the AMSU-B algorithm for RR according to Ferraro *et al.,* (2003) was this overestimation of stratiform situations. Another striking feature is that the rain rate determined by AMSU never exceeds 21 mm h^{-1}. This can easily be explained when looking at equation 2.19 again.

$$RR = a_0 + a_1\, IWP + a_2\, IWP^2 \tag{2.19}$$

The rain rate in this function is a quadratic product of IWP and the regression coefficients. The maximum rain rate can be calculated when:

$$\frac{dRR}{dIWP} = a_1 + 2a_2 IWP = 0 \tag{4.1}$$

From this last equation it can be observed that:

$$IWP = -\frac{1}{2}\frac{a_1}{a_2} \tag{4.2}$$

If we substitute this to equation 2.19, the maximum rain rate can be derived from the following simple equation:

$$RR_{\max} = a_0 - \frac{a_1^{\,2}}{4a_2} = 20.7 \tag{4.3}$$

By filling in the values for the regression coefficients from Table 2.2 we can calculate that the maximum rain rate is 20.7 mm h^{-1}. Note that the case studies presented in this study only have a CI of 1, and that a convective index of 3 (CI=3) will have a higher maximum rain rate of ~40 mm h^{-1}.

Following this comparison between the two methods it is also interesting to compare the effective diameter D_e obtained from AMSU measurements with the rain rate from Radar. In Figure 4.4 the values for rain rate from Radar and the effective diameter are plotted.

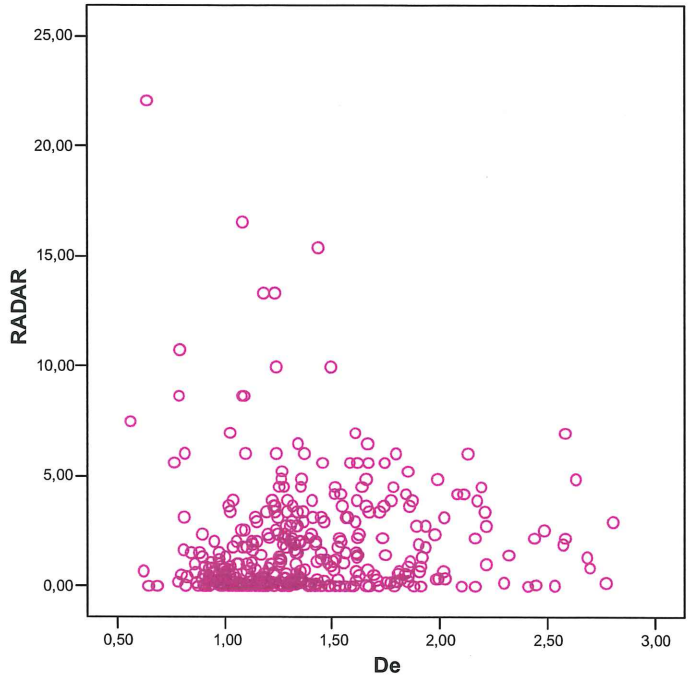

Fig. 4.4. The effective diameter D_e in mm (estimated by AMSU) plotted against rain rate by Radar in mm h^{-1}.

From Figure 4.4 we see that the ice particles with an effective diameter between 0.8 and 2.0 mm contribute most to rain. Most ice particles with an effective diameter smaller than 0.8 will evaporate before reaching the ground in a phenomenon called virga. It are these smaller particles that are also likely to grow within a cloud trough collision and coalescence with other particles. Ice particles with an effective diameter smaller than 0.4 mm are not detected by AMSU. The largest critical value for the ice particles is around 2.0 mm. When an ice particle has reached this size it will fall out of the cloud in the form of rain, hail or snow.

In Figure 4.3 we already saw there was a difference in the two methods. To statistically prove there is a significant difference in the two methods we need to calculate the correlation coefficient by using a Pearson test. By using a linear R^2 correlation-coefficient it shows that:

Table 4.1. Correlation of rain rate AMSU-B with Radar

	R^2	number of measurements
2003-04-26	0.0106	273
2003-05-05	0.1866	9
2003-09-10	0.0004	109
Total	0.0041	391

Combining the case studies (denoted as 'Total' in Table 4.1) it shows that less than 1% of the data of AMSU-B can be accounted for with the measurements of rain rate though Radar. From Figures 4.2 and 4.3 and from the results observed in Table 4.1 it can be concluded that there is a significant difference between the rain rates, which further implies the need to look at the algorithm again and calibrate it.

Since a calibration of D_e or IWP is not possible because no reference information is possible we will only look at the Goddard precipitation profile presented in section 2.3 for the calibration. The Goddard precipitation profile is presented in the form of equation 2.19 (Kummerow *et al.,* 1996, Ferraro *et al.,* 2003).

$$RR = a_0 + a_1\, IWP + a_2\, IWP^2 \qquad (2.19)$$

Following this equation we will recalculate the regression coefficients a_0, a_1 and a_2 by using the IWP's derived from AMSU-B and the RR's measured by Radar. For this calculation the data of all three case studies are combined. The values for a_0, a_1 and a_2 are:

Table 4.2. List of regression coefficients for validation.

	a_0	a_1	a_2
Total	2.760	-1.736	0.605

With these 'newly' calculated regression coefficients we can again compute the rain rate using the IWP in the form of equation 2.19. These results are again correlated with the rain rate from radar. The result of this correlation can be seen in Table 4.3

Table 4.3. Correlation of rain rate AMSU-B with Radar

	R^2
Total	0.0207

Although, the result of this correlation shows a higher value than Table 4.1, still only 2% of values of rain rate measured by Radar can be accounted for with IWP from AMSU. When Ferraro *et al.,* (2003) derived the regression coefficients for computing the rain rate using IWP data from NCEP stage IV data was used. In their validation it was shown that IWP correlated with the rain rate obtained from NCEP. However, following the results from Table 4.1, 4.2 and 4.3 it shows that IWP does not correlate with that rain rate measured by Radar.

4.2 Analysing using contingency table

A qualitative correlation between Radar and AMSU-B reveals there was no correlation between the two methods. Beside the lack of correlation, in qualitative term, we can also do a quantitative analysis to see if AMSU-B can accurately detect rain.

For both the Radar and AMSU-B we will first set an arbitrary threshold of 0.5 mm hr^{-1} which will indicate rain. Values below this threshold are depicted as dry. Both AMSU-B and Radar can than be simplified to a 1-0 statement (categorical observations), where a value of 1 depicts rain and 0 is depicted as dry (Table 4.4).

Table 4.4. The verification table for AMSU-B and Radar.

		Radar 1	0
AMSU	1	**H**	**F**
	0	**M**	**Z**

Let H be denoted as "hits", i.e. all correct observations of rain by AMSU-B and Radar. F is false alarms, i.e. all rain observed by AMSU-B, but not observed by Radar, M are the missed observations from AMSU, but observed by Radar and lastly Z, which depicts all correct no-observations.

The data of the three case studies is combined and we have altogether 3692 observations, with H+F+M+Z=3692. A perfect forecast sample is when F and M both are zero. The ratio of observed to non-observed cases (H+M)/(F+Z) is determined by the verification sample and is independent of the quality of observations. From the dataset we can calculate the following parameters:

- The Hit Rate; HR=(H+Z)/(H+M+F+Z), the fraction of perfect observations by AMSU-B when rain or no rain occurred.
- The False Alarm Rate; FAR=F/(F+Z), the fraction of observations by AMSU-B of rain when it did not occur.
- The Probability Of Detection; POD=H/(H+M), is the fraction of perfect observations of rain by AMSU-B.
- The Critical Success Index CSI=H/(H+M+F) which gives an indication of the overall performance of the method

If we then vary the threshold from 0.5 mm hr^{-1} to 2 mm hr^{-1}, with steps of 0.5 mm hr^{-1}, the following values for HR, FAR, POD and CSI are observed (Table 4.5).

Table 4.5. Values for HR, FAR, POD and CSI for increasing rain rate thresholds.

	0.5	1.0	1.5	2.0
HR	0.80	0.83	0.85	0.87
FAR	0.06	0.07	0.08	0.08
POD	0.27	0.30	0.31	0.33
CSI	0.22	0.22	0.20	0.18

From the results in Table 4.5 we see that AMSU gives a rather high hit rate (HR) when it comes down to identifying rain or no rain. This value is accompanied by a low value for FAR. The value for POD is low however. In around 30% of the cases AMSU is successful in identifying rain. Combining this result with HR and FAR it can be concluded that AMSU is more successful in detecting no rain, than it is in detecting rain. This conclusion is also visible in the figure of CSI, which is low. Especially this CSI gives a good idea of the overall performance of the method to identify rain with AMSU-B. In this study the method AMSU to detect rain or no rain in comparison to Radar is successful in 20% of the cases.

In the scatterplot of Figure 4.3 we already saw that the AMSU-B tends to overestimate the rain rate in comparison to the Radar. With this in mind we can do another quantitative analysis, by increasing the threshold for rain of AMSU-B from 1 mm hr^{-1} to 8 mm hr^{-1}. The threshold for rain measured by Radar will be kept at a constant of 0.5 mm hr^{-1}. In Table 4.6 the results for HR, FAR, POD and CSI can be observed for an increasing threshold for AMSU-B.

Table 4.6. Values for HR, FAR, POD and CSI for increasing AMSU-B RR thresholds.

	1.0	2.0	4.0	8.0
HR	0.80	0.80	0.80	0.80
FAR	0.06	0.06	0.06	0.06
POD	0.27	0.27	0.26	0.32
CSI	0.22	0.22	0.21	0.19

An increasing threshold shows a constant hit rate (HR) for the identification of rain using AMSU-B. Again, this high HR is accompanied by a low FAR. The CSI decreases when the threshold for AMSU is increased. This concludes that using AMSU-B to identify rain or not, in comparison to Radar, is successful in 20% of the cases. From Table 4.6 we can also see that both HR and FAR do not increase or decrease, which implies that AMSU overestimates the RR. This overestimation can also be observed when applying discrimination in the rain rate. For this discrimination only rain is identified and for both Radar and AMSU the following three classes will be identified:

1. Risk for/light precipitation

2. Light/moderate precipitation

3. Intensive precipitation.

So, instead of assigning a pixel with a value for the rain rate, it will rather be assigned a value for each of these three classes. In Table 4.5 and 4.6 we investigated if AMSU was able to detect rain and could discriminate between precipitation and no precipitation. When a discrimination in three classes is made we can see if AMSU is able to detect light, moderate or intensive precipitation. The thresholds which are used to discriminate between the three classes are:

Table 4.7. Classes of different precipitation intensities used in this investigation (Bennartz *et al.*, 1999).

class	type of precipitation	minimum rain rate	maximum rain rate
		[mm h^{-1}]	[mm h^{-1}]
1	Risk for/light precipitation	0.1	0.5
2	Light/moderate precipitation	0.5	5.0
3	Intensive precipitation.	5.0	30.0

The combined data set of Radar and AMSU is used and discrimination is made between these three classes. The results of this discrimination and the ability of AMSU to detect light, moderate or intensive precipitation can be seen in Table 4.8.

Table 4.8. Contingency table for the four different classes.

		AMSU			
R A D A R		measurements in class	class 1 [%]	class 2 [%]	class 3 [%]
	class 1	76	0.0	2.6	97.4
	class 2	197	0.5	7.6	91.9
	class 3	31	0.0	6.5	93.5

Ideally, if AMSU were successful in detecting light, moderate or intensive precipitation, as measured by Radar, the values on the diagonal all would be 100 %. However, we can see from Table 4.8 that this is not the case and that highest percentages can be found in AMSUs class 3. If the rain rate measured by Radar increases from class 1 onwards to class 3, AMSU still detects rain as being intensive precipitation (>5 mm hr^{-1}). This again confirms the overestimation of the rain rate by AMSU in comparison to Radar and also that AMSU is not able to detect light or moderate precipitation.

5. Discussion

In this study the retrieval of rain rate using AMSU-B over sea was omitted from the results. In this chapter we will describe what procedures should be followed in order to determine the rain rate above sea. Subsequently a discussion about the results will be presented in the form of an error analysis.

5.1 Estimating the upwelling brightness temperature at ice cloud bases above sea

In order to calculate the scattering parameters at 89 and 150 GHz. (Ω_{89} and Ω_{150}) information is needed from the brightness temperatures at cloud base. It was shown, that over land, the cloud-base brightness temperature could be estimated using an empirical relationship that exists between the AMSU lower and higher frequencies (Fig. 2.1). Zhao and Weng (2001) derived a relationship between AMSU-A and -B to retrieve the brightness temperatures at cloud base at 89 and 150 GHz in the form of Equations 2.7 and 2.8. Over sea however this relationship is not applicable. Weng and Grody (1998) derived the following relation for a scatterfree isothermal atmosphere to retrieve the brightness temperature (T_b) at cloud base above sea. It showed that T_b could be approximated by:

$$T_b = T_s[1-(1-\varepsilon)\Im^2] - \Delta T(1-\Im)[1+(1-\varepsilon)\Im \tag{5.1}$$

In this equation $\Im$ is the atmospheric transmittance, ε is the surface emissivity, T_s is the temperature at the surface, and ΔT is the difference in temperature between the surface and the atmospheric mean temperature. The atmospheric transmittance can be further expressed as:

$$\Im = \exp[-(\tau_o + \tau_v + \tau_l)/\mu] \tag{5.2}$$

Where τ_o, τ_v and τ_l are the optical thickness of oxygen, water vapour and cloud liquid water, respectively. It was pointed out by Weng and Grody (1998) that the brightness temperature estimated with the above equations contained less than 2% error. Thus, the brightness temperature of 89 and 150 GHz. at cloud bases $T_b(z_b,\mu)$ can be estimated using equation 5.1 with AMSU measurements at lower frequencies. However, the assumption was made that the brightness temperatures at lower frequencies are not affected by the presence of ice clouds. Note that the emissivity in equation 5.1 is a function of the surface temperature, wind speed, and salinity over oceans and can be computed using a previously developed model (Klein and Swift, 1977; Stogryn, 1972; Holinger, 1971). Here, τ_v is parameterised as a function of water vapour path, and τ_l is derived as a function of cloud liquid water and cloud layer temperature. In addition, τ_o is parameterised as a function of surface temperature (Weng *et al.,* 2000). Over oceans, the cloud liquid water and water vapour path can be retrieved directly from the AMSU lower frequencies (Grody *et al.,* 2001), whereas surface wind and temperature can be obtained through HIRLAM.

5.2 Error analysis

Several major sources of errors in retrieving cloud ice water path result from the uncertainties in the scattering parameters, bulk volume density, and effective particle diameter. The retrieval error of particle effective diameter is also directly dependent on the uncertainties in scattering parameters and bulk volume density.

5.2.1 Errors in bulk volume density

Provided that the bulk volume density of ice particles can be determined from other sources independently (i.e., assumed to be either a constant or a function of ice particle size), the IWP essentially only depends on the scattering parameters Ω and D_e. Because most published bulk density-size relations are derived for ice particles in nonprecipitating cirrus clouds, there are some uncertainties in using these relationships in the retrieval because the AMSU measurements are primarily sensitive to the precipitating ice clouds. An error of 30% in the density could result in an error of 25% in IWP and an error of 16% in RR (Fig. 5.1; Zhao and Weng, 2002). In this study a constant density of 600 $kg\ m^{-3}$ was used.

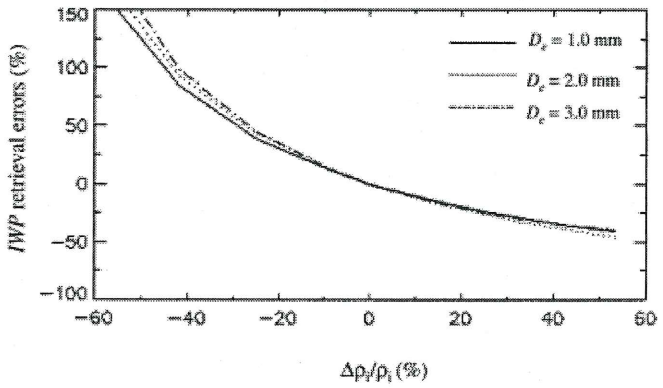

Fig. 5.1. The error in particle bulk volume density (Zhao and Weng, 2002).

5.2.2 Errors in retrieved effective diameter

As can be seen in Equation 2.16, the size of the effective ice particle is nonlinearly proportional to the scattering parameter ratio. The regression coefficients are also slightly dependent on the bulk volume density (Zhao and Weng, 2002). The error made in computing the effective diameter can be derived from equation 2.16 as follows:

$$\frac{\Delta D_e}{D_e} = g_1(D_e, r, \rho_i)\frac{\Delta r}{r} + g_2(D_e, r, \rho_i)\frac{\Delta \rho_i}{\rho_i} \tag{5.3}$$

with

$$\frac{\Delta r}{r} = h_1(T_{B0}, T_B) \times \left(\frac{\Delta T_{B0}}{T_{B0}} - \frac{\Delta T_B}{T_B} \right) \tag{5.4}$$

Where T_{B0} and T_B are the upwelling brightness temperatures at ice cloud base and top, respectively, and h_1 is a non-linear amplifying factor that is modulated by the scattering intensity of ice particles (Zhao and Weng, 2002). Note that the estimation of cloud base temperature (Fig 2.1; Eq. 2.14 and 2.15) is one of the major error sources in estimating the scattering parameter ratio. Figure 5.2a displays retrieved D_e error against the error in estimating the cloud-base brightness temperature. The error apparently increases linearly as the error of cloud-base brightness temperature increases.

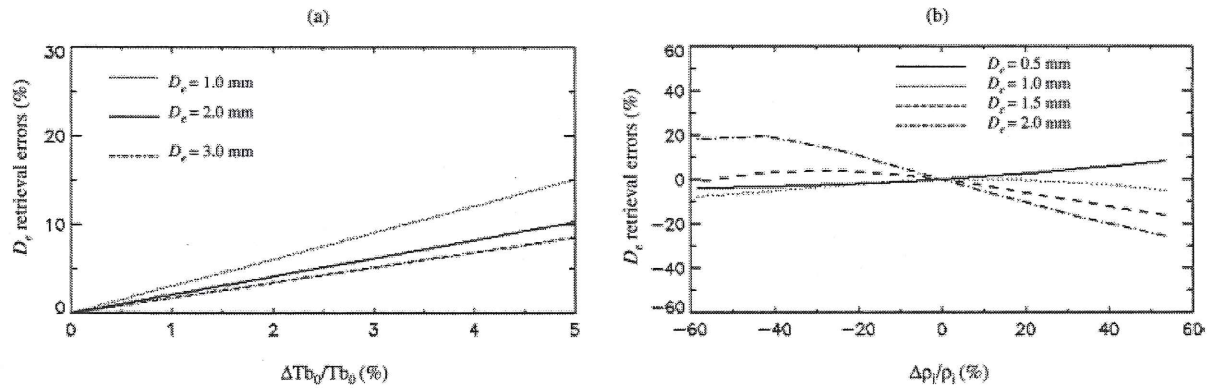

Fig. 5.2 The error of retrieved particle effective diameter due to (a) the error in estimating cloud-base brightness temperature and (b) the error in particle bulk volume density (Zhao and Weng, 2002).

The effect of cloud-base temperature error on the D_e retrieval is less significant for the larger ice particles. A 4.0-K error of the cloud-base temperatures results in a 5% retrieval error for D_e larger than 2.0 mm. The D_e retrieval error resulting from AMSU instrument noises (2 K) is less than 1% (Zhao and Weng, 2002). The second term of equation (5.3) represents the retrieval error due to the uncertainty in the particle bulk volume density used. As can be seen from Fig. 5.2b, for smaller D_e (<1.0 mm), the D_e error is less sensitive to the density error and is normally less than 5%. For a given error in the density, however, the retrieved D_e contains much larger errors at large size (Zhao and Weng, 2002).

5.2.3 Errors in retrieved cloud ice water path

From equation 2.12 we can see that the Ice Water Path (IWP) is a function of the ice particle effective diameter, the bulk volume density, and the scattering parameter. Its retrieval error can be derived as follows:

$$\frac{\Delta \mathrm{IWP}}{\mathrm{IWP}} = \frac{\Delta \Omega}{\Omega} + f_1(D_e, \rho_i)\frac{\Delta D_e}{D_e} + f_2(D_e, \rho_i)\frac{\Delta \rho_i}{\rho_i} \tag{5.5}$$

where

$$\frac{\Delta \Omega}{\Omega} = \frac{T_{B0}}{T_{B0} - T_B}\left(\frac{\Delta T_{B0}}{T_{B0}} - \frac{T_B}{T_B}\right) \tag{5.6}$$

From equation 5.5 the error in IWP is linearly related to the error of the scattering parameter but nonlinearly to the uncertainties in diameter and bulk density because the relationship between Ω_N and D_e is non-linear and depends on the particular ice particle size distribution and bulk volume density. As shown in equation 5.6 two major error sources result in the errors in scattering parameters. These include the errors in estimating cloud-base temperature and errors caused by instrument noise. For AMSU, the instrument noise is generally 2 K. This alone could introduce 3% – 10% of the errors in Ω for the brightness temperature depression ranging from 120 to 20 K (Zhao and Weng, 2002). Figure 5.3a shows the IWP error as a function of the error of the cloud-base brightness temperature.

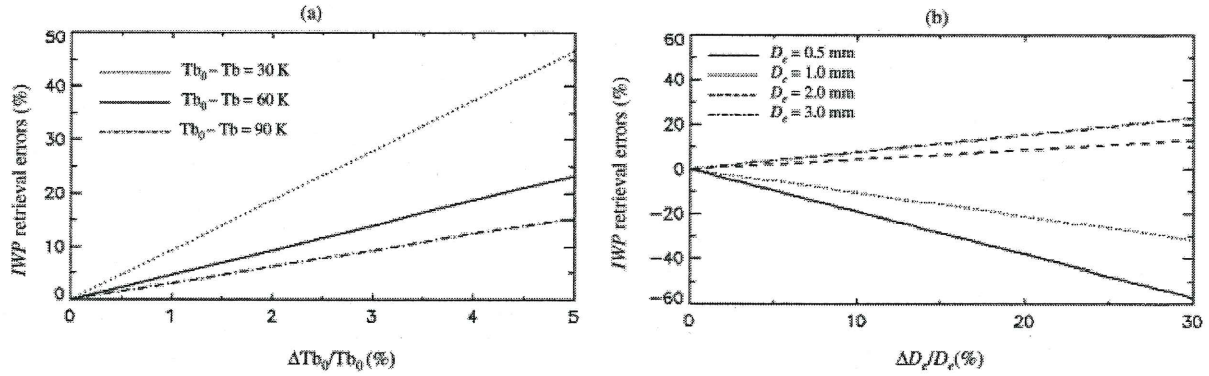

Fig. 5.3 The error of retrieved ice water path due to (a) the error in estimating cloud-base brightness temperature, (b) the error in retrieved diameter (Zhao and Weng, 2002)

The second term in equation 5.5 represents the error in IWP due to the uncertainty in the ice particle size. As shown in Fig. 5.3b, the error in IWP is directly proportional to the error of particle size. For a small particle size (<0.5 mm), Ω_N changes very rapidly with D_e. Thus, a small error in D_e would result in a large error in Ω_N or IWP. As D_e increases, Ω_N changes slowly with D_e and is less sensitive to the error in D_e. For 20% of D_e error, which is highly possible from the analysis of the previous paragraph, the error of IWP ranges from 10% to 20% for the particle size between 1.0 and 3.0 mm (see Fig. 5.3b; Zhao and Weng, 2002).

6. Conclusions

From the results presented in Chapter 4 we can conclude there exists a big difference between the two methods to retrieve the rain rate. When looking at the qualitative aspect no correlation between Radar and AMSU-B rain is observed. If we set Radar as a reference for the rain rate it reveals that AMSU-B tends to overestimate the rain rate. A lack of correlation between Ice Water Path and Radar also showed that the regression coefficients used in equation 2.19 could not be successfully recalculated again, in order to improve the correlation between AMSU-B and Radar. Combining the three case studies it was shown that only 2% of the values for rain rate could be accounted for with Radar.

A quantitative analysis confirms the conclusion that AMSU tends to overestimate the rain rate. High hit rates of 0.8 where observed. Meaning that 80% of observations of rain or no rain is detected by AMSU correctly. The probability of detection was around 30%, which implies that if it is raining, in 30% of the cases AMSU will detect this. The combination of this hit rate and the probability of detection can be described as the Critical Success Index, which was around 0.2. This means that AMSU-B successfully identifies rain in only 20% of the cases, in comparison to Radar. So, even though AMSU shows high hit rates, it is more successful in detecting no rain, than in rain. A discrimination in three classes of light, moderate and intensive precipitation showed that AMSU was not able to detect light or moderate precipitation but overestimated in such a way that all rain was interpreted as being intensive precipitation.

The lack in correlation of the qualitative aspect can best be explained when looking at the process of precipitation. Precipitation is the generic term for all liquid water or solid ice particles that are large enough to fall to the ground. The hydrometeors within a cloud contain all the liquid and ice particles. Only the hydrometeors that are large and heavy enough will fall out of the cloud and form rain. Some of the hydrometeors, however, will evaporate before reaching the ground. This phenomenon is called virga. A problem of the algorithm used in this study to retrieve the rain rate from AMSU-B is the fact that it does not correct sufficiently for this phenomenon. The algorithm expects that all ice particles with an effective diameter larger than 0.4 *mm* will subsequently produce rain. The ice particles that evaporate when falling to the surface will therefore also be included, which will subsequently cause an overestimation of the rain rate.

A difference is also present in which way both the method detects rain. The Doppler-Radar is situated on the surface and sends a beam through a cloud, which is reflected due to the presence of particles. More (bigger) particles mean more reflection. In this way the number of particles and their size can be measured more accurately and be translated into Radar. AMSU performs its measurements from a satellite and looks at a cloud from top. Due to a difference in scattering between cloud top and cloud base conclusions are made about the size of the particles and the number of particles with that size. In the error analysis we already concluded that these methods are highly sensitive to errors, especially in the estimation of the brightness temperature at cloud base. Also the difference in resolution between Radar and AMSU mean that errors made when calculating the RR with AMSU the error propagates and will subsequently mean an overestimation of the rain rate.

The usage of Radar as a reference also introduces additional errors in the comparison. First, because a perfect alignment in time of the weather Radar data with the passive microwave data cannot be obtained. Although the time difference between Radar data and AMSU-data was 10 minutes at maximum, rapidly developing thunderstorms may have significantly changed their state within this time frame. Secondly, the navigation of the satellite may introduce errors in the spatial collocation of the Radar and AMSU-data. Despite these problems Radar remains the only source to intercompare with AMSU on a pixel-by-pixel basis, since other observing systems as e.g. rain gauges are not capable to resolve the spatial and temporal distribution of the precipitation.

Although the retrieval of rain rate using AMSU-B was tested with NCEP-reanalysis and subsequently presented in literature in various articles, an ideal relation to the rain rate measured by Radar was not

observed in this study. More studies should address this relation in order to determine what weight should be put on the values for rain rate by using AMSU-B in future. The algorithm to retrieve the rain rate has changed in 2003 after a validation with NCEP Stage IV data (Ferraro, et al., 2003). The intention of changing the algorithm was to build a convective index (CI) into the algorithm, to overcome problems with under and overestimation of precipitation. From the results presented in this study it still shows that AMSU overestimates stratiform precipitation. More research should also address to this CI in future.

From the validation and calibration it showed that the IWP could not be correlated with the rain rate from Radar (Table 4.3). However, from Figure 4.4 a physical relation between the effective diameter (AMSU) and the rain rate from Radar was observed. If this retrieval of D_e (which is related to IWP) gives us reliable results, which can be explained physically with Radar measurements, how can it be that no correlation between IWP and Radar is observed? The most acceptable explanation has been given in section 5.2.3, where the errors made in the derivation of IWP were discussed. If future study could address these errors in retrieving IWP, a better correlation between IWP and RR of Radar would be detected. This would mean that the retrieval of rain rate from AMSU would probably also reveal a better correlation with Radar.

References

Bennartz, R., A. Thoss, et al. (1999). "Precipitation analysis from AMSU." *Swedish Meteorological and Hydrological Institute (SMHI), Norrköping, Sweden.* Website: http://www.smhi.se/saf/info.html

Doviak, R. and D.S. Zrnić, "Doppler Radar and Weather Observations". 2nd edition, *Academic Press*, San Diego, CA, 1993, 562 pp.

Ferraro, R., F. Weng, et al. (2003). "Advanced Microwave Sounding Unit (AMSU) cloud and precipitation algorithms." *Radio Sci.* **38(4)**: 8068.

Goodrum, G., K. B. Kidwel, et al. (1999). "NOAA KLM User's Guide." *NOAA.*

Grody, N., J. Zhao, et al. (2001). "Determinations of precipitable water and cloud liquid water over oceans from the NOAA 15 advanced microwave sounding unit." *J. Geophys. Res.* **106**: 2943-2953.

Holinger, J. P. (1971). "Passive microwave measuremnts of sea surface roughness." *IEEE Trans. Geosci. Elec.* **9GE**: 165-169.

Holleman, I. (2003). "Neerslaganalyse uit radar- en stationswaarnemingen" *KNMI*, IR-2003-06, Kon. Ned. Met. Inst., De Bilt.

Klein, L. A. and C. T. Swift (1977). "Emissivity for calm water." *IEEE Trans. Antennas Propag.*. **25**: 104-111.

Kummerow, C., W. S. Olson, et al. (1996). "A simplified scheme for obtaining precipitation and vertical hydrometeor profiles from passive micorwave sensors." *IEEE Trans. Geosci. Remote Sens.* **34**: 1213-1232.

Liou, K.N., (2002). "An introduction to Atmospheric Radiation.", 2nd edition, Academic Press, 593 pp.

Smith, E. A., J. Lamm, et al. (1998). "Results of the WetNet PIP-2 project." *J. Atmos. Sci.* **55**: 1483-1536.

Stogryn, A. (1972). "A study of radiometric emission from a rough sea surface." *NASA Contractor Rep.* **CR-2088**.

Ulbrich, C.W., (1983). "Natural variations in the analytical form of the rainsize distributions. " *J. Climate Appl. Meteor.* **22**: 1764-1775

Weng, F., (1992). "A multi-layer discrete-ordinate method for vector radiative transfer in a vertically-inhomogeneous, emitting and scattering atmosphere" Part I: Theory *J. Quant. Spec. Radiat. Trans.* **47**: 19-33

Weng, F., N. Grody, et al. (1997). "Cloud liquid water climatology derived from the Special Sensor Microwave Imager." *J. Clim.* **10**: 1086-1098.

Weng, F. and N. Grody (1998). "Physical retrieval of land surface temperature using the special sensor microwave imager." *J. Geophys. Res.* **103**: 8839-8848.

Weng, F. and N. Grody (2000). "Retrieval of ice cloud parameters using a microwave imaging radiometer." *J. Atmos. Sci.* **57**: 1069-1081.

Weng, F., R. Ferraro, et al. (2000). "Effects of AMSU cross-scan asymmetry of brightness temperatures on retrieval of atmospheric and surface parameters" *Microwave Radiometry and Remote Sensing of the Earth's Surface and Atmosphere.*: 255-262.

Weng, F., L. Zhao, et al. (2003). "Advanced Microwave Sounding Unit (AMSU) cloud and precipitation algorithms." *Radio Science.* **38**: 8086-8096.

Zhao, L. and F. Weng (2001). "Retrieval of ice cloud parameters using the Advanced Microwave Sounding Unit (AMSU)." *J. Appl. Meteor.* **41**: 384-395.

Zhao, J., F. Weng, et al. (2003). "Precipitation Retrievals using both AMSU Window and Sounding Channels." NOAA/NESDIS/ORA, Camp Springs, MD 20746., Website: http://orbit-net.nesdis.noaa.gov/arad2/MSPPS/index.html

Appendix A

C-program to read and calculate the rain rate from AMSU-A and AMSU-B data.

```
#include <stdio.h>
#include <string.h>
#include <math.h>

#include "description.h"
#include "data.h"

#define MAXLINE 300

int difdtg_(int*,int*,int*,int*);
int adddtg_(int*,int*,int*,int*,int*);
int fgetcBE(FILE *);
int print_help(void);
float latlon2dist(float,float,float,float);
float berDe();

/* functions */
struct HEADER read_aapp_header(FILE *);
struct LINEDATA *read_aapp_data(FILE *,struct HEADER);

/* externals */
int debug=0;
int header=0;
int info=0;

int writePPM=0;
int writeAMSA=0;
int writePOS=0;
int writeRAT=0;
int writeANG=0;
int writeDe=0;

float De;
float RAT;
float Pi;

float a0=-0.300323;
float a1=4.30881;
float a2=-3.98255;
float a3=2.78323;

float b0=-0.294459;
float b1=1.38838;
float b2=-0.753624;

float c0=-1.19301;
float c1=2.08831;
float c2=-0.857469;

float e0=0.321717;
float e1=16.5043;
float e2=-3.3419;

float f0=0.08925;
float f1=20.8194;
float f2=-2.9117;

float IWP;
float W;
float Wn;
```

```
float RR;

int AmsuAline;
int AmsuBline;
int AmsuAlon;

int AmsuBlon;
int AmsuAlat;
int AmsuBlat;

int main(int argc, char **argv) {
 FILE *fpa,*fpb,*fpc;

 struct HEADER AmsuAhead, AmsuBhead;
 struct LINEDATA *AmsuAdata, *AmsuBdata;

 char ppmFile[30];

 int i;
 int ia;
 int j;
 int ja;

 int i0,j0;
 int r,g,b;

 float mindist;
 float dist,dist1,dist2,dist3,dist4,dist5;

 int kmin;
 int *index;
 int value;
 int CI;

 float bt89;
 float bt150;
 float w89;
 float w150;
 float ratio;
 float mu;

 float D1;
 float D2;
 float D3;

 int channel=0;
 int line;

 if (argc==1) print_help();
 if (!strcmp(argv[1],"-h")) print_help();


 if (!(fpa=fopen(argv[1],"r"))) {
  fprintf(stderr,"Cannot open %s for reading!\n",argv[1]);
  return(1);
 }

 if (!(fpb=fopen(argv[2],"r"))) {
  fprintf(stderr,"Cannot open %s for reading!\n",argv[2]);
  return(2);
 }

 if (!(fpc=fopen("20030505.txt","w")))
 { printf("error while opening rr.txt file");
   return(1);}

 /* options */
```

```
i=2;
while (++i<argc) {
  if (!strcmp(argv[i],"-i")  ) { info=1; }
  if (!strcmp(argv[i],"-d")  ) { debug=1; }
  if (!strcmp(argv[i],"-d1")  ) { debug=2; }
  if (!strcmp(argv[i],"-H")  ) { header=1; }
  if (!strcmp(argv[i],"-c")  ) { channel=atoi(argv[i+1]); }
  if (!strcmp(argv[i],"-ppm")  ) { writePPM=1; strcpy(ppmFile,argv[i+1]);}
  if (!strcmp(argv[i],"-amsa")  ) { writeAMSA=1; strcpy(ppmFile,argv[i+1]);}
  if (!strcmp(argv[i],"-pos")  ) { writePOS=1; }
  if (!strcmp(argv[i],"-rat")  ) { writeRAT=1; }
  if (!strcmp(argv[i],"-ang")  ) { writeANG=1; }
  if (!strcmp(argv[i],"-De")  ) { writeDe=1; }
}
/* read header AMSUA*/
AmsuAhead=read_aapp_header(fpa);
/* read data ASMUA*/
AmsuAdata=read_aapp_data(fpa,AmsuAhead);

/* read header AMSUB*/
AmsuBhead=read_aapp_header(fpb);
/* read data AMSUB*/
AmsuBdata=read_aapp_data(fpb,AmsuBhead);

fclose(fpa);fclose(fpb);

if (info) {
  fprintf(stderr,"# satellite %i\n",AmsuBhead.satid);
  fprintf(stderr,"# time : ");
  fprintf(stderr,"%i:%06i - ",AmsuBhead.startDate,AmsuBhead.startTime);
  fprintf(stderr,"%i:%06i\n",AmsuBhead.endDate,AmsuBhead.endTime);
  fprintf(stderr,"# Number of channels %i \n",AmsuBhead.nchannel);
  fprintf(stderr,"# Number of obs %i (%ix%i)\n",
          AmsuBhead.scnlin*AmsuBhead.nangle,AmsuBhead.scnlin,AmsuBhead.nangle);

  fprintf(stderr,"# total obs time %i\n\n",

difdtg_(&AmsuBhead.startDate,&AmsuBhead.startTime,&AmsuBhead.endDate,&AmsuBhead.endTime));
 }

if (debug==1 && AmsuAhead.instrument==AMSUA) {
  for(i=0;i<AmsuAhead.nchannel;i++)
    printf("freq channel %i = %s\n",i,freqAMSUA[i]);
}
if (debug==1 && AmsuBhead.instrument==AMSUB) {
  for(i=0;i<AmsuBhead.nchannel;i++)
    printf("freq channel %i = %s\n",i,freqAMSUB[i]);
}


if (writePOS) {
  for(line=0;line<AmsuBhead.scnlin;line++)
    for(i=0;i<AmsuBhead.nangle;i++)
        printf("%12.5f %12.5f %7.3f\n",
            AmsuBdata[line].lat[i],AmsuBdata[line].lon[i],
            AmsuBdata[line].bt[i][channel]);
}

if (writeRAT) {
  for(line=0;line<AmsuBhead.scnlin;line++){
    RAT=AmsuBdata[line].bt[i][0]/AmsuBdata[line].bt[i][1];
  }
}

if (writeANG) {
  for(line=0;line<AmsuBhead.scnlin;line++)
    printf("%12.5f\n",
```

```
            AmsuBdata[line].loczen[i]);
}

  /* De rain rate wordt uitgerekend en in een PPM file geschreven */

if (writePPM) {
  if (!(fpb=fopen(ppmFile,"w"))) {
    fprintf(stderr,"Cannot open %s for writing!\n",ppmFile);
    return(1);
  }
  fprintf(fpb,"P5\n%i %i\n255\n",AmsuBhead.nangle,AmsuBhead.scnlin);
}
index=(int *)(malloc(90*AmsuBhead.scnlin*sizeof(int)));

/* de procedure om afstanden te berekenen tussen AmsuA en AmsuB begint hier */

ia=0;
for (i=0;i<AmsuBhead.scnlin;i++)
  for (j=0;j<AmsuBhead.nangle;j++) {
    mindist=9999;
    /*for (ia=0;ia<AmsuAhead.scnlin;ia++)*/
    /*for (ja=0;ja<AmsuAhead.nangle;ja++) {*/
    dist1=9999;
    dist2=9999;
    dist3=9999;
    dist4=9999;
    dist5=9999;
    dist=9999;
    ja=j/3;

    /* 5 afstanden worden berekend; ia,ja met i,j */
    /* en vervolgens door ia en ja met resp =1 en -1 te verlagen */
    /* berekenen we ook die afstanden */

    dist1=latlon2dist(AmsuAdata[ia].lat[ja],
                      AmsuAdata[ia].lon[ja],
                      AmsuBdata[i].lat[j],
                      AmsuBdata[i].lon[j]);

    if((ia-1)>=0){
        dist2=latlon2dist(AmsuAdata[ia-1].lat[ja],
                          AmsuAdata[ia-1].lon[ja],
                          AmsuBdata[i].lat[j],
                          AmsuBdata[i].lon[j]);
    }
    if((ia+1)<AmsuAhead.scnlin){
        dist3=latlon2dist(AmsuAdata[ia+1].lat[ja],
                          AmsuAdata[ia+1].lon[ja],
                          AmsuBdata[i].lat[j],
                          AmsuBdata[i].lon[j]);
    }
    if((ja-1)>=0){
        dist4=latlon2dist(AmsuAdata[ia].lat[ja-1],
                          AmsuAdata[ia].lon[ja-1],
                          AmsuBdata[i].lat[j],
                          AmsuBdata[i].lon[j]);
    }
    if((ja+1)<AmsuAhead.nangle){
        dist5=latlon2dist(AmsuAdata[ia].lat[ja+1],
                          AmsuAdata[ia].lon[ja+1],
                          AmsuBdata[i].lat[j],
                          AmsuBdata[i].lon[j]);

    }

    /* tweede stap is te controleren en te kijken welke afstand */
    /* de korste is. Als voor dist-X dit het geval is, wordt kmin */
```

```
/* berekend en opgeslagen */

if (dist1<=dist) {
        dist=dist1;
                kmin=(AmsuAhead.nangle*(ia)+ja);
}
if (dist2<=dist) {
        dist=dist2;
        kmin=(AmsuAhead.nangle*(ia-1)+ja);
}

if (dist3<=dist) {
        dist=dist3;
        kmin=(AmsuAhead.nangle*(ia+1)+ja);
}

if (dist4<=dist) {
        dist=dist4;
        kmin=(AmsuAhead.nangle*(ia)+(ja-1));
}
if (dist5<=dist) {
        dist=dist5;
        kmin=(AmsuAhead.nangle*(ia)+(ja+1));
}

/* het print statement is ter controle */

/* fprintf(stderr,"i=%d,j=%d,ia=%d,ja=%d,dist=%12.5f %d\n",*/
/* i,j,ia,ja,dist,AmsuAhead.scnlin); */

index[(i*AmsuBhead.nangle)+j]=kmin;


/* de afstanden zijn bekend. Verdere berekening van RR */

value=index[(i*AmsuBhead.nangle)+j];

ja=value%AmsuAhead.nangle;
ia=(value/AmsuAhead.nangle);

if ((AmsuBdata[i].bt[j][0]>0)&&
   (AmsuBdata[i].bt[j][1]>0)&&
   (AmsuBdata[i].bt[j][2]>0)&&
   (AmsuBdata[i].bt[j][3]>0)&&
   (AmsuBdata[i].bt[j][4]>0)&&
   (AmsuAdata[ia].bt[ja][0]>0)&&
   (AmsuAdata[ia].bt[ja][1]>0)) {

        bt89=17.88+(1.61*(AmsuAdata[ia].bt[ja][0]))-
  (0.67*(AmsuAdata[ia].bt[ja][1]));
         bt150=33.78+(1.69*(AmsuAdata[ia].bt[ja][0]))-
  (0.80*(AmsuAdata[ia].bt[ja][1]));


w89=(bt89-(AmsuBdata[i].bt[j][0]))/(AmsuBdata[i].bt[j][0]);
w150=(bt150-(AmsuBdata[i].bt[j][1]))/(AmsuBdata[i].bt[j][1]);

if ((w89>0.01)&&(w150>0.02)){
ratio=w89/w150;
} else {
ratio=0;
}

if (0.2<ratio && ratio<=1.0){
  De=a0+(a1*ratio)+(a2*(ratio*ratio))+(a3*(ratio*ratio*ratio));
if (De<=1.) {
        Wn=exp(b0+(b1*(log(De)))+(b2*((log(De))*(log(De)))));
```

```
    } else {
          Wn=exp(c0+(c1*(log(De)))+(c2*((log(De))*(log(De)))));
    }
    W=(w150-w89)/w89;
    Pi=4*atan(1.);
    mu=cos((AmsuBdata[i].loczen[i]/180.)*Pi);
    IWP=mu*De*0.6*(W/Wn);

    If ((IWP>=0.05)&&(De>0.4)) {

    D1=(AmsuBdata[i].bt[j][2])-(AmsuBdata[i].bt[j][4]);
    D2=(AmsuBdata[i].bt[j][3])-(AmsuBdata[i].bt[j][4]);
    D3=(AmsuBdata[i].bt[j][2])-(AmsuBdata[i].bt[j][3]);

    if ((D2>-2)&&(D2>D1)&&(D2>D3)){
          CI=1;
    }
    if ((D2>0)&&(D1>0)&&(D3>0)&&(D1>D3)&&(D2>D3)){
       CI=2;
    }
    if ((D2>0)&&(D1>0)&&(D3>0)&&(D1>D3)&&(D2<D3)){
       CI=3;
    }

    if ((CI==1)||(CI==2)) {
      RR=e0+(e1*IWP)+(e2*(IWP*IWP));
    }
    if (CI==3) {
          RR=f0+(f1*IWP)+(f2*(IWP*IWP));
    }
    if (RR<0) {
          RR=0;
    }
    if (RR>30) {
          RR=30;
    }

    if (writePPM) fprintf(fpb,"%c",(char)(AmsuBdata[i].bt[j][1]-150));
    else {
          /*if (RR>0)*/
          fprintf(fpc,"%f %f %f %f %f %f %f %f %f %f\n",
          AmsuBdata[i].lon[j],
          AmsuBdata[i].lat[j],
          AmsuAdata[ia].bt[ja][0],
          AmsuAdata[ia].bt[ja][1],
          AmsuBdata[i].bt[j][0],
          AmsuBdata[i].bt[j][1],
           w89,w150,IWP,RR);
     }
    }/* if (ratio< */
   }
  }
 }

 fclose (fpc);
 if (writePPM) fclose(fpb);

}
```

Appendix B

C-program to project rain rate from Radar on AMSU-B grid.

```
#include <stdio.h>
#include <string.h>
#include <math.h>

#define MAXLINE 300

float latlon2dist(float,float,float,float);

/* externals */
int debug=0;

int a,b,k,value,nread;

int i;
int ia;
int j;
int ja;

int c;
int nr;

float *avgRR;
int *ntimes;
float *totalRR;

int nia, ni, nj;

float dist1, dist2;
float mindist;
float junk;

typedef struct READER
  {
  float lat, lon, RR;
  }READ;

READ *RAD, *AMSU;

typedef struct distance
 {
 int i; /* radar i-pixel */
 int j; /* radar j-pixel */
 int ia;/* index in AMSU */
 }distan;

distan *grid;
int value=0;


int main()
{

/* Open the RADAR and the AMSU-file */

FILE *f1, *f2;
char string[256];

int i0,j0,imin;

if ((f1=fopen("rad0910.txt","r"))==NULL) {
  fprintf(stderr,"Error opening ascii-file : %s\n","RAD0910.txt");
```

```
  exit(1);
}

if ((f2=fopen("20030910.txt","r"))==NULL){
  fprintf(stderr,"Error opening ascii-file : %s\n","20030910.txt");
  exit(1);
}
fprintf(stderr,"opening ascii-file : %s\n","RAD0910.txt"); fprintf(stderr,"opening ascii-file : %s\n","20030910.txt");

/* Read the data of the RADAR-file */
/* allocate memmory */
RAD=(READ*) malloc(256*256*sizeof(READ));

for (a=0;a<12;a++){
   fgets(string,255,f1);
}

fprintf(stderr,"header skipped\n");
a=0;
while (fgets(string,255,f1)!=NULL && !feof(f1)){
   sscanf(string,"%f%f%f",&RAD[a].lon,&RAD[a].lat,&RAD[a].RR);
   a++;
}


/* Read the data of the AMSU-file */
/* allocate memmory */
AMSU=(READ*) malloc(256*256*sizeof(READ));

b=0;
i=0;
j=1;
while (fgets(string,255,f2)!=NULL && !feof(f2)){
 sscanf(string,"%f%f%f%f%f%f%f%f%f%f",&AMSU[b].lon,&AMSU[b].lat,&junk,
            &junk,&junk,&junk,&junk,&junk,&junk,&AMSU[b].RR);
  if (i%90==0) {
            if (49<=AMSU[b].lat && AMSU[b].lat<=55) j=1; /* read DATA */
            else j=0;
  }
  if (j==1) b++;
  i++; /* total number read from AMSU */
}

fprintf(stderr,"AMSU read = %i\n",b);
nr=b;

/*for(i=0;i<b;i++)
   printf("ASMU %f %f %f: RAD %f %f %f\n",
            AMSU[i].lon,AMSU[i].lat,AMSU[i].RR,RAD[i].lon,RAD[i].lat,RAD[i].RR);
*/
/* Zowel a als b moeten omgeschreven worden naar grid met i,j (ia,ja) */


/* start van het berekenen van de distances tussen de gridpunten */

/* Allocate memory*/
/* In Grid we will place the i,j of radar and the nearest ia of AMSU */

   grid=(distan*) malloc(256*256*sizeof(distan));

  totalRR=(float*) malloc(nr*sizeof(float));
  ntimes=(float*) malloc(nr*sizeof(int));

  for(i=0;i<nr;i++){
            totalRR[i]=0.0;
            ntimes[i]=0;
  }
```

```
  for (i=0;i<256;i++){
   for (j=0;j<256;j++){
          mindist=9999;
          /* afstanden worden berekend; ia met i,j */
          for(ia=0;ia<b;ia++) {
                        dist1=latlon2dist(
                                RAD[i+j*256].lat,RAD[i+j*256].lon,
                                AMSU[ia].lat, AMSU[ia].lon);
                        if (ia>=0 && ia<b && dist1<mindist){
                                mindist=dist1;
                                ja=ia; /* kleinste afstand */
                        } /* if (dist1<mindist) */
                } /* for(ia=0;ia<b;ia++) */
          imin=ja;
          if ((RAD[i+j*256].RR >= 0) && (RAD[i+j*256].RR < 30)){
                ntimes[imin]++;
                totalRR[imin]+=RAD[i+j*256].RR;
          } /*if(RAD[i+j*256].RR < 30){*/


      grid[value].i=i;
          grid[value].j=j;
          grid[value].ia=ia;
          value++;
          /*fprintf(stderr,"%i %i %i\n",i,j,ia);*/
    }/*     for (j=0;j<256;j++)*/
  }/* for (i=0;i<256;i++)*/


/* Start the procedure to calculate the average RR from Radar on AMSU grid */

  avgRR=(float *)(malloc(nr*sizeof(float)));

  for(imin=0;imin<nr;imin++) {
          if ( ntimes[imin]>0) {
                avgRR[imin]=totalRR[imin]/(float)ntimes[imin];
                printf("%f %f %f %f\n",
                AMSU[imin].lon,AMSU[imin].lat,
                AMSU[imin].RR,avgRR[imin]);
      } /* if (ntimes */
  }

  /*printf("avgRR=%f\n",avgRR[nia]);*/

fclose(f1);
fclose(f2);
}

/*}*/
/*exit(0);*/
```

Eerder gepubliceerde titels in de reeks *Intern Rapport*:

2000-01	Inventarisatie nowcasting-technieken voor gevaarlijk weer : eindrapport / *G.T. Geertsema, A. Maas, H.R.A. Wessels, H. Benschop, B. Blaauboer en C.J. Kok*
2000-02	COST-76 : aims, achievements and future / *W.A. Monna*
2000-03	Verslag van een studiereis naar de National Weather Service van de USA, juni 2000 / *A.W. Donker*
2000-04	Definitiestudie vervanging IBDS : eindrapport / *Sylvia Barlag, Hans Roozekrans, Richard Rothe, Jan Bijma, Jan Jans en Frans Debie*
2000-05	Rapportage voorstudie herinrichting Cabauw / *Projectgroep Voorstudie Herinrichting Cabauw*
2001-01	Neerslagonderzoek / *Foeke Kuik*
2001-02	Estimation of the maximum velocity of convective wind gusts / *Iwan Holleman*
2001-03	Synoptisch Waarneemnet Nederland 2000 (SWaNet NL 2000) / *J.P. van der Meulen*
2001-04	Eindrapport AutoTrend "Automatische generatie TREND'S" / *Albert Jacobs*
2002-01	Sensitivity of the MAECHAM4 model to imposed ozone distributions / *Anne Grete Straume, Elisa Manzini and Peter Siegmund*
2002-02	Kwaliteitscriteria AVW / *H.R.A. Wessels*
2002-03	SAFIR beeldproduct voor real-time gebruik / *Iwan Holleman*
2003-01	LITE4ADM : on the use of LITE data for the Atmospheric Dynamics Mission Aeolus / *G.J. Marseille, A. Stoffelen en A. van Lammeren*
2003-02	Mistdetectie met satellietbeelden / *Peter Baas*
2003-03	Gecombineerde weergave van AMDAR en METAR / *O. van der Velde, I. Holleman, J. van der Meulen en S. Barlag*
2003-04	Three events of strong deep moist convection in The Netherlands / *P. Groenemeijer*
2003-05	KNMI HFDS data format specification, v. 3.5 / *H. Roozekrans and I. Holleman*
2003-06	Neerslaganalyse uit radar- en stationswaarnemingen / *I. Holleman*
2003-07	Synthetic water vapour images from the HIRLAM model using a radiative transfer model / *M.H. Voogt*
2003-08	Temperature advection derived from Doppler radar wind profiles / *Susanne Jonker*
2004-01	KNMI-project "Visie Waarnemingen op Land Water Overgangen Nederland (WOLWO NL) : eindrapport / *Henk Benschop, Albert Klein Tank en Ad de Ruiter*
2004-02	Retrieval of rain rate using AMSU measurements / *Jarno Schipper*